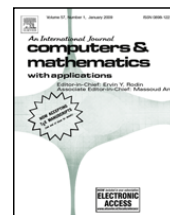




Contents lists available at ScienceDirect

## Computers and Mathematics with Applications

journal homepage: [www.elsevier.com/locate/camwa](http://www.elsevier.com/locate/camwa)Criterion of numerical instability of liquid state in LBE simulations<sup>☆</sup>

Alexander L. Kupershtokh

Lavrentyev Institute of Hydrodynamics of Siberian Branch of Russian Academy of Sciences, Lavrentyev Prosp. 15, Novosibirsk, 630090, Russia

## ARTICLE INFO

## Keywords:

Lattice Boltzmann equation method  
Equation of state  
Phase transition  
Stability of LBE simulations

## ABSTRACT

The numerical stability of the lattice Boltzmann equation (LBE) method in simulations of a fluid described by an equation of state with possible vapor–liquid phase transitions is considered. The Courant–Friedrichs–Lewy number defined by the advection term in the Boltzmann equation is exactly equal to unity in classical LBE models. However, this condition does not ensure the numerical stability of LBE simulations with the equation of state. In our numerical LBE simulations, we find out that instability arises initially in the liquid phase, even if the vapor phase and, consequently, the vapor–liquid interface are absent. We demonstrate both in numerical tests and theoretically that the numerical stability of LBE simulations requires the criterion  $\tilde{c} \leq \tilde{c}_{cr}$  to be fulfilled for the liquid phase, where  $\tilde{c} = c_s \Delta t / h$  is the hydrodynamic Courant number. The hydrodynamic Courant number is proportional to the speed of sound  $c_s$ , obtained from an equation of state of a fluid. This criterion is very similar to the well-known criteria of numerical stability of explicit finite difference schemes for a compressible fluid. The critical value of the Courant number  $\tilde{c}_{cr}$  depends neither on the temperature  $T$ , nor on the fluid velocity, nor on the form of the equation of state. This critical value is equal to  $\tilde{c}_{cr} = 1.1547$  for the kinetic temperature of LBE pseudo-particles  $\tilde{\theta} = 1/3$ .

© 2009 Elsevier Ltd. All rights reserved.

## 1. Introduction

The well-known hydrodynamic equations for a viscous compressible fluid are the continuity equation

$$\frac{\partial \rho}{\partial t} + \nabla(\rho \mathbf{u}) = 0, \quad (1)$$

and the Navier–Stokes equation

$$\frac{\partial(\rho u_i)}{\partial t} + \frac{\partial \Pi_{ij}^{(0)}}{\partial x_j} = \rho a_i + \frac{\partial}{\partial x_j} \left( \mu \left( \frac{\partial u_i}{\partial x_j} + \frac{\partial u_j}{\partial x_i} \right) \right) + \frac{\partial}{\partial x_j} \left( \left( \lambda - \frac{2}{3} \mu \right) \delta_{ij} \frac{\partial u_k}{\partial x_k} \right). \quad (2)$$

Here,  $\rho$  is the density of a fluid,  $\mathbf{u}$  is the velocity of a fluid flow,  $\mathbf{F} = \rho \mathbf{a}$  is the body force,  $\mu$  and  $\lambda$  are the dynamic and second viscosities,  $\Pi_{ij}^{(0)} = P(\rho, T) \delta_{ij} + \rho u_i u_j$  is the non-viscous part of the momentum flux tensor, and  $\delta_{ij}$  is the Kronecker delta.  $P(\rho, T)$  is the equation of state that allows the vapor–liquid phase transition. Two boundary conditions should be satisfied at each element  $S$  of interfaces between phases of densities  $\rho'$  and  $\rho''$ . The first condition is the kinematic condition  $\mathbf{u}'' = \mathbf{u}'$

<sup>☆</sup> This work was supported in part by the Russian Foundation for Basic Research (grant No. 06-08-01006) and by the Siberian Branch of the Russian Academy of Sciences (grant No. 116-2009).

E-mail address: [skn@hydro.nsc.ru](mailto:skn@hydro.nsc.ru).

if the mass flux through the interface is absent. The second condition is the dynamic condition

$$\begin{aligned}(\sigma_{ij}'')_{\tau} &= (\sigma_{ij}')_{\tau} + \nabla\gamma|_S, \\ (\sigma_{ij}'')_n - (\sigma_{ij}')_n &= -\gamma(T) \left( \frac{1}{R_1} + \frac{1}{R_2} \right),\end{aligned}$$

where  $(\sigma_{ij})_n$  and  $(\sigma_{ij})_{\tau}$  are the components of the stress tensor  $\sigma_{ij}$  normal and tangential to the interface,  $\gamma(T)$  is the surface tension, which depends on temperature in the general case,  $R_1$  and  $R_2$  are the radii of curvature of the interface. The stress tensor is equal to

$$\sigma_{ij} = -P\delta_{ij} + \mu \left( \frac{\partial u_i}{\partial x_j} + \frac{\partial u_j}{\partial x_i} \right) + \left( \lambda - \frac{2}{3}\mu \right) \delta_{ij} \frac{\partial u_k}{\partial x_k}.$$

In LBE methods, different phases of a substance are usually simulated as one fluid. In this case, there is no need to track the interfaces between the vapor and liquid phases. These interfaces are represented as thin transition layers of finite width (several lattice nodes) in which the density changes smoothly from one bulk value to another. For the purpose of simulating the transition between phases, special forces between neighbor nodes were included into the LBE algorithm [1,2]. These forces implicitly simulated the vapor–liquid coexistence curve and also the surface tension at the interface.

In this article, we consider the numerical stability of the class of lattice Boltzmann equation (LBE) models that can simulate the fluid described by an equation of state (EOS) with possible vapor–liquid phase transitions.

In classical LBE simulations, the Courant–Friedrichs–Lewy (CFL) number, which is defined by the advection term in the Boltzmann equation, is exactly equal to unity. However, this condition does not ensure the numerical stability of LBE simulations with the equation of state. In our numerical LBE simulations, we found that instability arises initially in the liquid phase because of a higher speed of sound in the liquid in comparison with the vapor phase (in accordance with the equation of state). Moreover, the numerical instability of the liquid phase can arise in LBE simulations at relatively low temperatures, even if the liquid–vapor interface layers are absent.

For every temperature lower than the critical temperature  $T_{cr}$ , the gas and the liquid states of different densities can coexist simultaneously. Two boundaries of these phases on the temperature–specific volume diagram (as well as on the  $T$ – $\rho$ ,  $P$ – $v$ , and  $P$ – $\rho$  diagrams) can be called the gas and liquid branches of the binodal curve, respectively. These branches separate the regions of the gas and the liquid states from the regions of metastable states. In their LBE simulations, many authors cannot reproduce the binodal curve for different EOS at temperatures far below the critical point. They encounter such difficulties because of the numerical instability of simulations [3]. Hence, a relatively low ratio of liquid to vapor densities ( $\rho_L/\rho_V \leq 10^3$ ) is possible and can be obtained if some EOS was used in the LBE simulations [2–5]. Moreover, in their works [3–5], the binodal curve on the temperature–specific volume phase diagram (especially the vapor branch) at low temperatures considerably differs from the theoretical binodal curve obtained from the equation of state using the Maxwell rule.

It would seem obvious that the numerical algorithm of LBE simulations should be stable in the broadest possible range of temperatures, and the coexistence curve obtained in simulations should coincide with the theoretical curve in the broadest range of temperatures as well.

All of the problems mentioned above arise because these variants of LBE simulations are stable only in a narrow range of temperatures (not far from the critical point). These problems were solved in our previous works [6–9] and the ratio of liquid to vapor densities was attained to the level up to  $10^9$  in the stationary case [6]. For this purpose, we proposed to use:

- method of exact difference [10,7] for the implementation of the body force term,
- specific form of approximation of the potential gradient on a lattice [6,8], and
- relatively small  $\Delta t/h$  ratio, required for numerical stability of the LBE algorithm (preliminary analysis was carried out in [6]).

This paper is organized as follows. In Section 2, we describe in detail the variant of the LBE method for simulating a fluid with possible liquid–vapor phase transitions in accordance with the equation of state  $P(\rho, T)$ . Section 3 is devoted to defining the criterion of numerical stability for a liquid phase of initially uniform density: The criterion of numerical stability for the liquid phase is obtained both theoretically and in numerical tests. Section 4 outlines our conclusions. The details of an analytical derivation of the stability criterion are described in Appendix.

## 2. Lattice Boltzmann equation method

In the lattice Boltzmann method, the fluid is represented by a collection of pseudo-particles that move on a regular spatial lattice and undergo collisions at its nodes. We use the usual evolution equation with the BGK (single relaxation time) collision operator

$$N_k(\mathbf{x} + \mathbf{e}_k, t + \Delta t) = N_k(\mathbf{x}, t) + \frac{N_k^{\text{eq}}(\rho(\mathbf{x}, t), \mathbf{u}(\mathbf{x}, t)) - N_k(\mathbf{x}, t)}{\tau} + \Delta N_k, \quad (3)$$

where  $\mathbf{e}_k = \mathbf{c}_k \Delta t$  are the lattice vectors (vectors to the neighbor nodes),  $\Delta t$  is the time step, and  $\Delta N_k$  is the change of distribution functions that occurs because of the action of the body force.

The discrete set of velocity vectors  $\mathbf{c}_k$  depends on the lattice geometry. In our tests, we use the standard one-dimensional LBE model D1Q3 with three velocity vectors  $|\mathbf{c}_k| \in \{0, h/\Delta t\}$  and the standard two-dimensional model D2Q9 with nine velocity vectors  $|\mathbf{c}_k| \in \{0, h/\Delta t, \sqrt{2}h/\Delta t\}$  on a square lattice [11]. Here,  $h$  is the lattice spacing.

The fluid density  $\rho$  and the velocity  $\mathbf{u}$  at a node are calculated as

$$\rho = \sum_k N_k, \quad \rho \mathbf{u} = \sum_k \mathbf{c}_k N_k. \tag{4}$$

We use the equilibrium distribution functions in the standard form

$$N_k^{\text{eq}}(\rho, \mathbf{u}) = \rho w_k \left( 1 + \frac{\mathbf{c}_k \mathbf{u}}{\theta} + \frac{(\mathbf{c}_k \mathbf{u})^2}{2\theta^2} - \frac{\mathbf{u}^2}{2\theta} \right), \tag{5}$$

where  $\theta$  is the “kinetic temperature” of pseudo-particles in LBE models. For the standard “isothermal” LBE models D1Q3, D2Q9 and D3Q19 [11] with the equilibrium distribution (5), the “kinetic temperature” is equal to  $\theta = (h/\Delta t)^2/3$ . The values of coefficients  $w_k$  can be found in [11]. They are equal to  $w_0 = 2/3, w_{1,2} = 1/6$  for D1Q3 model and  $w_0 = 4/9, w_{1-4} = 1/9, w_{5-8} = 1/36$  for D2Q9 model.

For the body force term, we used the method of exact difference [10,7]

$$\Delta N_k = N_k^{\text{eq}}(\rho, \mathbf{u} + \Delta \mathbf{u}) - N_k^{\text{eq}}(\rho, \mathbf{u}), \tag{6}$$

where the change of velocity

$$\Delta \mathbf{u} = \mathbf{F} \Delta t / \rho \tag{7}$$

is defined by the force  $\mathbf{F}$  acting on the node.

In [10,7], the method of exact difference was derived directly from the Boltzmann equation

$$\frac{\partial f}{\partial t} + \boldsymbol{\xi} \nabla f + \mathbf{a} \nabla_{\boldsymbol{\xi}} f = \Omega, \tag{8}$$

where  $\boldsymbol{\xi}$  is the microscopic velocity of molecules,  $f(\mathbf{x}, \boldsymbol{\xi}, t)$  is the distribution function in the phase space  $(\mathbf{x}, \boldsymbol{\xi})$ , and  $\mathbf{a} = \mathbf{F}/\rho$  is the acceleration due to the action of the body force. At a low Knudsen number  $\varepsilon$ , the perturbation method can be applied for the distribution function  $f(\mathbf{x}, \boldsymbol{\xi}, t) = f^{\text{eq}}(\rho, \boldsymbol{\xi}, \mathbf{u}) + \varepsilon f^{(1)} + \varepsilon^2 f^{(2)} + \dots$ . In the first approximation that is usually used in other methods, we have  $\nabla_{\boldsymbol{\xi}} f \approx \nabla_{\boldsymbol{\xi}} f^{\text{eq}}$ . For example, the explicit expression was obtained directly from (5) in this approximation [12,13]

$$\mathbf{a} \nabla_{\mathbf{u}} f^{\text{eq}} = - \frac{\mathbf{a}(\boldsymbol{\xi} - \mathbf{u})}{\theta} f^{\text{eq}} \tag{9}$$

that is often used in LBE simulations. Unfortunately, this formula has only the first order in  $\Delta \mathbf{u} = \mathbf{a} \Delta t$  after discretization in time and velocity space. Hence, it is applicable only at rather low values of body forces.

On the one hand, we noticed that the equality  $\nabla_{\boldsymbol{\xi}} f^{\text{eq}}(\rho, \boldsymbol{\xi}, \mathbf{u}) = -\nabla_{\mathbf{u}} f^{\text{eq}}(\rho, \boldsymbol{\xi}, \mathbf{u})$  is valid because any form of the equilibrium distribution function can depend only on the difference  $(\boldsymbol{\xi} - \mathbf{u})$  to ensure the Galilean invariance. On the other hand, we use the mathematical identity

$$\nabla_{\mathbf{u}} f^{\text{eq}} \cdot \frac{d\mathbf{u}}{dt} = \left. \frac{df^{\text{eq}}(\rho, \mathbf{u})}{dt} \right|_{\rho=\text{const}} \tag{10}$$

for every fixed value of  $\boldsymbol{\xi}$ . This full derivative of the equilibrium distribution function  $f^{\text{eq}}(\rho, \mathbf{u})$  should be calculated at constant density  $\rho$  in a frame of reference that moves with the fluid velocity  $\mathbf{u}$ .

Therefore, the body force term  $\mathbf{a} \nabla_{\boldsymbol{\xi}} f$  in the Boltzmann equation (8) can be rewritten using a full derivative of the equilibrium distribution function along the Lagrange coordinate  $df^{\text{eq}}(\rho, \boldsymbol{\xi}, \mathbf{u})/dt$  at a fixed  $\boldsymbol{\xi}$  and a constant density  $\rho$ . Hence, Eq. (8) takes the approximate form

$$\frac{\partial f}{\partial t} + \boldsymbol{\xi} \nabla f = \Omega + \left. \frac{df^{\text{eq}}(\rho, \mathbf{u})}{dt} \right|_{\rho=\text{const}}. \tag{11}$$

The condition of constant density refers only to the full derivative. This circumstance does not mean at all that the density  $\rho$  should be constant in time during the process of simulations. After discretizing Eq. (11) in time and velocity space, we derived the method of exact difference for LBM in the form (6). A more detailed discussion about the advantages of this method and an analysis comparing it with other implementations of the body force term in LBE simulations can be found in works [6–9].

In general, body forces include all forces (external and internal) that act on small volumes of a fluid. In particular, they include forces acting between neighbor nodes that were introduced for the purpose of simulating multiphase flows [1,2].

In these works, different phases are simulated by only one set of distribution functions  $N_k$  at each node. In this case, there is no need to track the interfaces between the phases of a substance. This method of multiphase simulation is similar to the well-known shock-capturing method for simulating fluid flows with shock waves.

For the classical LBE method without any interaction forces between neighbor nodes, it is well known that the non-viscous part of the momentum flux tensor in macroscopic hydrodynamic equations obtained from the Chapman–Enskog expansion of the LBE method has the form  $\Pi_{ij}^{(0)} = \rho\theta\delta_{ij} + \rho u_i u_j$  with the gaseous equation of state  $P = \rho\theta$ . In work [2], Zhang and Chen proposed to introduce the total force acting on every node from the neighbor nodes as a gradient of a special potential

$$\mathbf{F}(\mathbf{x}, t) = -\nabla U(\mathbf{x}, t). \tag{12}$$

To reproduce an arbitrary equation of state  $P(\rho, T)$ , Zhang and Chen proposed to choose the potential  $U$  in the form [2]

$$U = P(\rho, T) - \rho\theta. \tag{13}$$

In this case, the non-viscous part of the momentum flux tensor in macroscopic hydrodynamic equations obtained from the Chapman–Enskog expansion of the LBE method takes a desired form  $\Pi_{ij}^{(0)} = P(\rho, T)\delta_{ij} + \rho u_i u_j$ . A more detailed explanation can be found in work [2].

Our variant of the LBE method [6,8,9] is the generalization of the method given by Zhang and Chen [2]. The continuity and Navier–Stokes equations, obtained using the Chapman–Enskog expansion of our variant of the LBE algorithm, have the form [2,7]

$$\frac{\partial \rho}{\partial t} + \frac{\partial(\rho u_i^*)}{\partial x_i} = 0, \tag{14}$$

$$\begin{aligned} \frac{\partial(\rho u_i^*)}{\partial t} + \frac{\partial \Pi_{ij}^{(0)*}}{\partial x_j} = & \rho a_i + \nu \frac{\partial}{\partial x_j} \left( \rho \left( \frac{\partial u_i}{\partial x_j} + \frac{\partial u_j}{\partial x_i} \right) \right) + \nu \frac{\partial}{\partial x_j} \left( u_i \frac{\partial \rho}{\partial x_j} + u_j \frac{\partial \rho}{\partial x_i} \right) \\ & + \left( \tau - \frac{1}{2} \right) \Delta t \frac{\partial}{\partial x_j} \left( u_i u_j \frac{\partial \rho}{\partial t} \right). \end{aligned} \tag{15}$$

Here  $\nu = \theta(\tau - 1/2)\Delta t$  is the kinematic viscosity and  $\mathbf{a} = \mathbf{F}/\rho$ . The redefined velocity vector  $\mathbf{u}^*$  is specified at a half time step  $\Delta t/2$  as  $\rho \mathbf{u}^* = \sum_k \mathbf{c}_k N_k + \mathbf{F}\Delta t/2$  [14]. The momentum flux tensor  $\Pi_{ij}^{(0)*}$  in (15) is also rewritten for the redefined velocity. Two last extraneous terms in (15) are the deviations of the Chapman–Enskog expansion for the LBE models from the Navier–Stokes equation in the case of a compressible fluid. The last term has the third order of smallness in  $u$  because  $\partial \rho / \partial t \sim u$ . Obviously, these terms practically do not influence the numerical stability of the liquid phase that is initially close to uniform. In this case, the initial perturbations of density and velocity are small. The tests of numerical stability of the LBE algorithm confirm that these extraneous terms do not influence the criterion of the numerical stability of the liquid phase. For almost incompressible fluids, these terms are usually small. However, for fluids with vapor–liquid interface layers (compressible fluids), which are not at rest ( $\mathbf{u} \neq 0$ ), these terms are very important. Therefore, we take them into account in LBE simulations [7]. We do so in a finite difference form as a negative addition to the body force term [7].

In the model offered by Zhang and Chen [2], the physical temperature  $T$  was introduced using the equation of state in the form  $P(\rho, T)$ . They used the conventional energy equation in a finite difference form. In the present paper, we do not use the energy equation to test the stability of the LBE model. Therefore, the temperature  $T$  cannot be more complicated than the predefined function of coordinates and time. In every run of the test for investigation of the numerical stability of the LBE method, the temperature  $T$  is a parameter constant in space and time. The temperature  $T$  varies in the range from  $T = 0.1T_{cr}$  to  $T = 1.1T_{cr}$  (Fig. 2), where  $T_{cr}$  is the value of the temperature at the critical point.

### 3. The numerical instability of the liquid phase in LBE simulations

This section of the article is devoted to defining the criterion of numerical instability of the liquid phase in LBE simulations (without interfaces with vapor). The liquid of uniform density  $\rho_0$  is initially at rest. In one-dimensional simulations, periodic boundary conditions in  $x$  direction are used. In two-dimensional simulations, periodic boundary conditions in both  $x$  and  $y$  directions are used.

For the fluid, we use anyone of the equations of state: van der Waals, Carnahan–Starling or Kaplun EOS (modified) [6,8]. All these equations of state describe the possible vapor–liquid phase transitions if the fluid temperature is lower than the critical temperature. We use the equations of state written in reduced variables  $\tilde{P} = P/P_{cr}$ ,  $\tilde{\rho} = \rho/\rho_{cr}$  and  $\tilde{T} = T/T_{cr}$ , where  $P_{cr}$ ,  $\rho_{cr}$ , and  $T_{cr}$  are the values of pressure, density, and temperature at the critical point. For example, the van der Waals equation of state, written in reduced variables, has the form

$$\tilde{P} = \frac{8\tilde{\rho}\tilde{T}}{3 - \tilde{\rho}} - 3\tilde{\rho}^2. \tag{16}$$

It is convenient to use the reduced variables not only for the equation of state, but also for the LBE distribution functions  $\tilde{N}_k = N_k/\rho_{cr}$  and for the velocity  $\tilde{\mathbf{u}} = \mathbf{u}\Delta t/h$ .

The evolution equation (3) in reduced variables has the form

$$\tilde{N}_k(\mathbf{x} + \mathbf{c}_k \Delta t, t + \Delta t) = \tilde{N}_k(\mathbf{x}, t) + \frac{\tilde{N}_k^{\text{eq}}(\tilde{\rho}, \tilde{\mathbf{u}}(\mathbf{x}, t)) - \tilde{N}_k(\mathbf{x}, t)}{\tau} + \Delta \tilde{N}_k. \quad (17)$$

The equilibrium distribution (5) can be rewritten in reduced variables as

$$\tilde{N}_k^{\text{eq}}(\tilde{\rho}, \tilde{\mathbf{u}}) = \tilde{\rho} w_k \left( 1 + \frac{\tilde{\mathbf{c}}_k \tilde{\mathbf{u}}}{\tilde{\theta}} + \frac{(\tilde{\mathbf{c}}_k \tilde{\mathbf{u}})^2}{2\tilde{\theta}^2} - \frac{\tilde{\mathbf{u}}^2}{2\tilde{\theta}} \right), \quad (18)$$

where  $\tilde{\theta} = \theta(\Delta t/h)^2 = 1/3$  is the dimensionless “kinetic” temperature of LBE pseudo-particles. The reduced density  $\tilde{\rho}$  and velocity  $\tilde{\mathbf{u}}$  are found from the following expressions:

$$\tilde{\rho} = \sum_k \tilde{N}_k, \quad \tilde{\rho} \tilde{\mathbf{u}} = \sum_k \tilde{\mathbf{c}}_k \tilde{N}_k. \quad (19)$$

The body force term (6) in reduced variables has the form

$$\Delta \tilde{N}_k = \tilde{N}_k^{\text{eq}}(\tilde{\rho}, \tilde{\mathbf{u}} + \Delta \tilde{\mathbf{u}}) - \tilde{N}_k^{\text{eq}}(\tilde{\rho}, \tilde{\mathbf{u}}), \quad (20)$$

where

$$\Delta \tilde{\mathbf{u}} = \tilde{\mathbf{F}}/\tilde{\rho} = -\tilde{\nabla} \tilde{U}/\tilde{\rho} \quad (21)$$

is the reduced change of velocity. Here,  $\tilde{\nabla}$  is the gradient in the space of dimensionless coordinates  $\tilde{\mathbf{x}} = \mathbf{x}/h$ . The potential  $U$  should be also written in reduced form  $\tilde{U} = U(\Delta t/h)^2/\rho_{\text{cr}}$ . Therefore, we have

$$\tilde{U} = k\tilde{P}(\tilde{\rho}, \tilde{T}) - \tilde{\rho}\tilde{\theta}. \quad (22)$$

Here, the dimensionless coefficient

$$k = \frac{P_{\text{cr}}}{\rho_{\text{cr}}} \left( \frac{\Delta t}{h} \right)^2 \quad (23)$$

plays an important role in the stability of simulations. For real fluids and a reasonable choice of the ratio  $h/\Delta t$ , this parameter is usually small. For example, if we take  $h/\Delta t = 10^3$  m/s, then  $k \approx 0.01$  for argon and for several other fluids.

Earlier, for Eq. (12) (in the reduced variables (21)), we proposed the specific form of the finite difference approximation of the gradient of the potential  $\tilde{U}$  on the lattice [6,8] using a single free parameter  $A$

$$\tilde{\mathbf{F}}(\mathbf{x}) = \frac{1}{\alpha h} \left[ A \sum_k \frac{G_k}{G_0} \Phi^2(\mathbf{x} + \mathbf{e}_k) \mathbf{e}_k + (1 - 2A) \Phi(\mathbf{x}) \sum_k \frac{G_k}{G_0} \Phi(\mathbf{x} + \mathbf{e}_k) \mathbf{e}_k \right], \quad (24)$$

where

$$\Phi^2(\mathbf{x}) = -\tilde{U}(\mathbf{x}). \quad (25)$$

Obviously, the value of  $\Phi(\mathbf{x})$  can be defined from (25) only in the region of fluid states in which the potential (22) is negative  $\tilde{U} \leq 0$ . The coefficients  $G_k$  are different for basic and diagonal directions of the lattice. The coefficients for the diagonal directions  $G_k$  are equal to  $G_0/4$  and  $G_0/2$  for the two-dimensional model D2Q9 and the three-dimensional model D3Q19, respectively. These values ensure the isotropy of (24) in space.

This approximation of mesoscopic forces (12) better describes the binodal curve defined by the equation of state. For example, for the van der Waals equation of state at  $A = -0.152$ , the values of density of the liquid and vapor phases obtained in LBE simulations coincide with the theoretical values on the binodal curve. Their accuracy is better than 0.4% in the range from the critical point  $T = T_{\text{cr}}$  down to  $T = 0.4T_{\text{cr}}$  [6,8,9]. Moreover, for the potential in form (25), the approximation (24) at  $A = 0$  represents the method proposed by Shan and Chen but modified for the EOS in the form  $P(\rho, T)$  (see [6,8]).

Examples of instability of the liquid phase are shown in Fig. 1 both for the one-dimensional (a) and two-dimensional (b) tests. In both cases, the initial states of the liquid are near the boundary of stability. Thus, the oscillations appear after a long time. The tests show the oscillations of the fluid velocity to be similar.

We performed a standard linear stability analysis of our numerical LBE algorithm (17)–(22) theoretically in a way similar to [15,16]. For this purpose, the growth of small harmonic perturbations of density  $\rho = \rho_0 + A_0 \exp(ikx)$  and velocity  $u = u_0 + B_0 \exp(ikx)$  is considered (see details in Appendix). The criterion of stability is obtained in the form

$$\tilde{c}^2 - \tilde{\theta} \leq 1, \quad (26)$$

where  $\tilde{\theta} = 1/3$  for the equilibrium distribution (5). Here  $\tilde{c} = c_s \Delta t/h$  is the dimensionless speed of sound and can be called the hydrodynamic Courant number [15,16], where  $c_s = \sqrt{\partial P/\partial \rho}$  is the speed of sound that is defined by the equation of

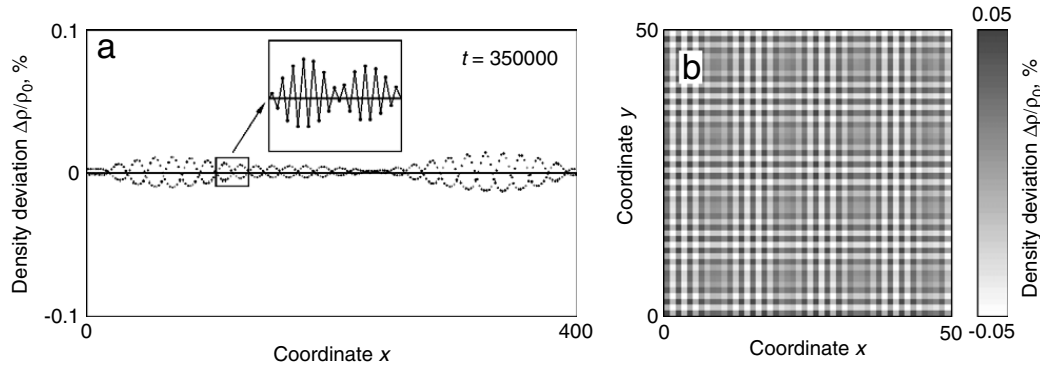


**Fig. 1.** Numerical instability of the liquid phase. The density deviations  $\Delta\rho/\rho_0$  are shown. (a) One-dimensional test of model D1Q3,  $\tilde{T} = 0.6$ ,  $\tilde{\rho}_0 = 2.692$ ,  $\tilde{c} = 1.166$ ,  $t = 350,000$  time steps. (b) Two-dimensional test of model D2Q9,  $\tilde{T} = 0.8$ ,  $\tilde{\rho}_0 = 2.645$ ,  $\tilde{c} = 1.168$ ,  $t = 125,000$  time steps.

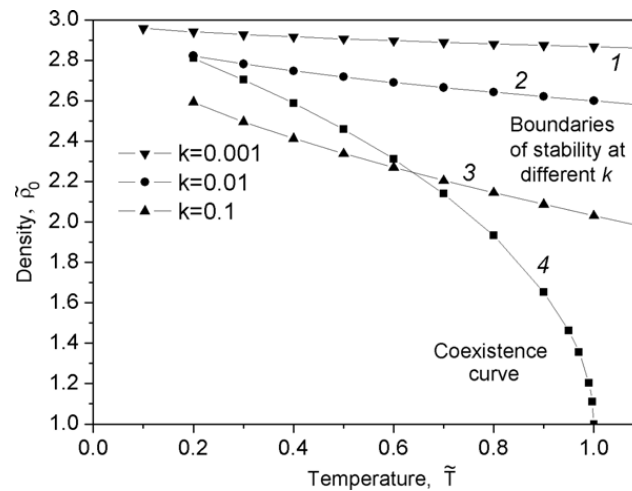


**Fig. 2.** Boundaries of numerical stability of the LBE algorithm for different  $k$  (curves 1, 2, 3) and the liquid branch of the binodal curve (curve 4) obtained both theoretically and in the LBE simulations [6,8] for the van der Waals EOS.

state. The criterion of stability (26) could be written in an equivalent and simpler form  $\tilde{c} \leq \tilde{c}_{cr}$ , where the critical value of the hydrodynamic Courant number is  $\tilde{c}_{cr} = \sqrt{1 + \tilde{\theta}} = 1.1547$  for  $\tilde{\theta} = 1/3$ .

The Courant–Friedrichs–Lewy (CFL) number defined by the advection term in the Boltzmann equation is exactly equal to unity in classical LBE simulations ( $\mathbf{e}_k = \mathbf{c}_k \Delta t$ ). However, one can see that this number does not ensure the stability of LBE simulations with an arbitrary equation of state.

In LBE simulations, we found the boundaries of numerical stability of the initially uniform fluids with the density  $\tilde{\rho}_0$  and initial velocity  $\mathbf{u}_0 = 0$ . These boundaries of numerical stability at different values of the reduced temperature  $\tilde{T}$  and for three values of the dimensionless coefficient  $k$  (0.001, 0.01, and 0.1) are shown in Fig. 2 (curves 1, 2, and 3, respectively). Curve 4 is the boundary of liquid states on the temperature–density phase diagram (the liquid branch of the binodal curve). The state  $\tilde{\rho}_0 = 1$ ,  $\tilde{T} = 1$  is the critical point.

If the density of the liquid lies above the boundary of stability, the numerical stability is absent. For example, at  $k = 0.1$  (relatively large time step  $\Delta t$ ), all states of the liquid on the binodal curve at the temperatures  $\tilde{T} < 0.65$  are unstable. Therefore, the coexistence of the liquid and vapor phases cannot be simulated for these temperatures at  $k = 0.1$ .

In the reduced variables form, we have the speed of sound squared  $\tilde{c}^2 = k \partial \tilde{P} / \partial \tilde{\rho}$ . Thus, it is possible to vary the hydrodynamic Courant number by changing the time step  $\Delta t$  and lattice spacing  $h$  in expression (23) for the parameter  $k$ .

All points of these boundaries of instability obtained in LBE simulations (Fig. 2) at different temperatures and different values of  $k$  correspond well to the critical value of the hydrodynamic Courant number obtained theoretically (Fig. 3, curve 1). For a wide range of parameters (relaxation time, initial perturbations, size of calculation area, waiting time, etc.), the numerical instability arises at values of the hydrodynamic Courant number greater than the critical one (Fig. 3). The values of the expression  $(\tilde{c}^2 - \tilde{\theta})$  obtained in all numerical tests are shown in Fig. 4. These data include the results obtained in test with the initial fluid velocity  $u = 0.2$  and in two-dimensional tests with the D2Q9 LBE model. All data correspond well to the unified boundary of instability, defined by the theoretical criterion (26). Thus, the critical value of the hydrodynamic Courant number depends neither on the temperature, nor on the velocity of the fluid, nor on the parameter  $k$ , nor on the form of the equation of state.

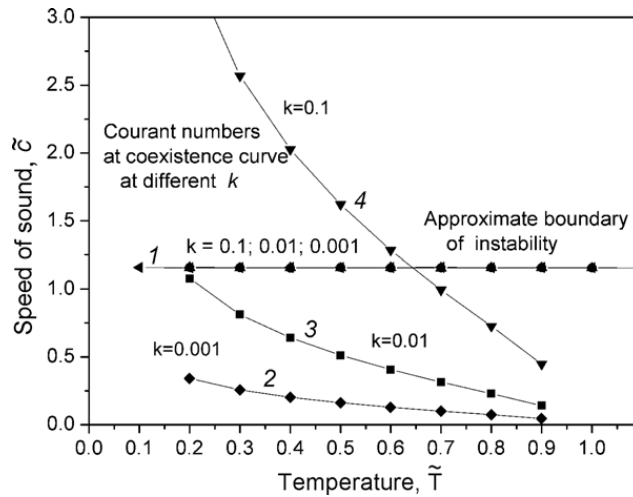


Fig. 3. Curve 1 is the universal boundary of numerical instability of the LBE algorithm obtained in computer simulations at different values of the parameter  $k$ . Curves 2, 3, and 4 show the values of  $\tilde{c}$  on the liquid branch of the binodal curve (see Fig. 2, curve 4) at  $k = 0.001, 0.01, \text{ and } 0.1$ , respectively.

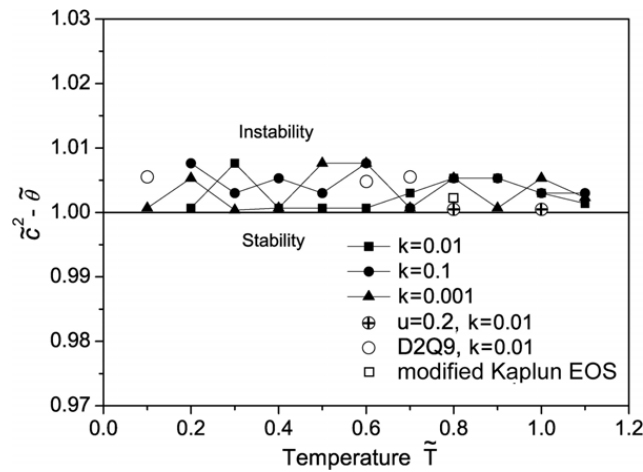


Fig. 4. The map of numerical stability for the D1Q3 and D2Q9 LBE models with the equation of state in the form  $P(\rho, T)$ . The boundary of stability corresponds to  $(\tilde{c}^2 - \tilde{\theta}) = 1$ . All other data are the results of the numerical tests that correspond to instability of initial states. The black signs are the results of one-dimensional tests with initial conditions for the fluid  $\mathbf{u} = 0$  and  $\rho = \text{const}$ . The open box is the value obtained for the modified Kaplun equation of state. The circles with a cross are the results of one-dimensional tests for the initial velocity  $\mathbf{u} = 0.2$ . The open circles are the results of two-dimensional tests with the D2Q9 LBE model.

The following consideration offers a possible explanation for this phenomenon. The Chapman–Enskog expansion of the lattice Boltzmann equation method results in the Euler equations in the first order of expansion and the Navier–Stokes equations in the second order of expansion [7]. Therefore, the lattice Boltzmann equation method simulates the hydrodynamic behavior of a compressible fluid for which the hydrodynamic Courant number is the usual criterion of the numerical stability for explicit finite difference schemes [15,16].

As mentioned above, the value of  $\Phi(\mathbf{x})$  can be defined from (25) only in the region of fluid states in which the potential (22) is negative. For example, for the van der Waals EOS (16), the condition  $\tilde{U} \leq 0$  is satisfied in the whole region of numerical stability of the LBE algorithm (see Fig. 2) at  $k = 0.1$  for  $\tilde{T} \leq 1.2$ , at  $k = 0.01$  for  $\tilde{T} \leq 4$ , and at  $k = 0.001$  for  $\tilde{T} \leq 30$  (see Fig. 5). For the van der Waals EOS, the condition  $\tilde{U} \leq 0$  is fulfilled in the gaseous phase at  $\tilde{\rho} \rightarrow 0$  if  $8k\tilde{T} < 1$ .

#### 4. Conclusions

The numerical stability of multiphase LBE simulations using the method proposed in [8,9] is limited mainly by the stability of calculations in the liquid phase, for which the speed of sound is a sharply increasing function of density. The criterion of stability of the liquid phase (26) is obtained theoretically for the one-dimensional D1Q3 LBE model. Obviously, this criterion does not depend on a specific equation of state. The numerical instability arises in the liquid phase at values of the hydrodynamic Courant number  $\tilde{c} = c_s \Delta t / h$  above the critical value  $\tilde{c}_{cr}$ . For the LBE models considered in this paper, the critical value is equal to 1.1547 for  $\tilde{\theta} = 1/3$ . The same results are obtained in numerical tests both for the D1Q3 and for two-dimensional D2Q9 models. Hence, the criterion obtained is valid for a wide range of LBE models often used in LBE simulations. The critical value of the hydrodynamic Courant number depends neither on the temperature  $T$ , nor on the fluid velocity, nor on the parameter  $k$ , nor on the form of the equation of state. It is obvious that the criterion of stability of the

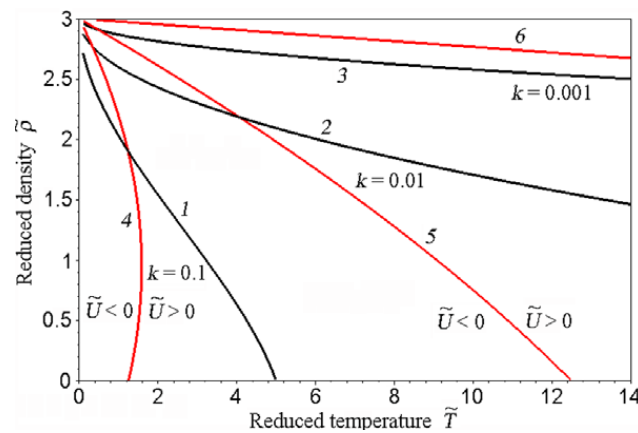


**Fig. 5.** Boundaries of numerical stability of the LBE algorithm for different  $k$  (curves 1, 2, and 3). Curves 4, 5, and 6 show the lines  $\tilde{U} = 0$  for different  $k$ . All curves were calculated for the van der Waals equation of state at  $\tilde{\theta} = 1/3$ .

liquid phase described here does not depend on the way in which the dimensionless variables are constructed. Our scheme, which we proposed in [8,9], ensures the computational stability at a very large density ratio (up to  $10^9$  in the stationary case [6] with  $k \leq 0.01$ ) and reproduces the binodal curve on the temperature–volume phase diagram for an arbitrary EOS very accurately.

**Appendix**

The purpose of this Appendix is to provide details in the derivation of the criterion of numerical stability (26) of the LBE algorithm in which the equation of state in the form  $P(\rho, T)$  is used.

We carry out theoretically the standard linear stability analysis of our numerical LBE algorithm in a similar way as it was done for finite difference equations in [15,16]. In the Appendix, all variables are in the reduced form as in Section 3. We consider the D1Q3 model with the velocity vectors  $\tilde{c}_k \in \{0, 1, -1\}$ . For this model, the growth of small amplitude harmonic perturbations of density  $\tilde{\rho} = \tilde{\rho}_0 + A \exp(ikx)$  and velocity  $\tilde{u} = \tilde{u}_0 + B \exp(ikx)$  is theoretically analyzed. Moreover, the case  $\tilde{u}_0 = 0$  is considered, for which all formulas can be written in a relatively compact form.

The eigenvalues  $\lambda_i$  of the transition matrix  $G$  can be found from the eigenvalue equation

$$\det(G - \lambda E) = 0, \tag{27}$$

where  $E$  is the unit matrix. The numerical algorithm is stable if moduli of all eigenvalues of (27) are smaller than or equal to 1 for all real values of the parameter  $k$ .

The algorithm of the LBE method (17)–(25) described in Section 3 consists of several steps. One of the advantages of the exact difference method for the implementation of the body force term is the exact commutative property of this operator with the BGK (single relaxation time) collision operator [7]. This feature is also confirmed in numerical tests. All other steps of the LBE method can also be interchanged in reasonable order.

For convenience of analytical consideration of the numerical stability of the LBE algorithm, we use the following sequence of the four steps:

- (1) Calculations of the changes (20) of the distribution functions that arise because of the action of the body forces (21) between the neighbor nodes using potential (22).
- (2) Advection step.
- (3) Collision step with a single relaxation time operator.
- (4) Calculations of new values of density and velocity (19).

The initial values of the distribution functions  $\tilde{N}_k(x, t)$  are defined by the initial perturbations. In the case of small perturbations, the equilibrium distribution (18) can be used in the linear approximation with respect to perturbation amplitudes

$$\tilde{N}_k^{\text{eq}} = \tilde{\rho} w_k + \tilde{\rho}_0 w_k (\tilde{\mathbf{c}}_k \tilde{\mathbf{u}}) / \tilde{\theta}. \tag{28}$$

Here, the values of the coefficients are  $\tilde{\theta} = 1/3$ ,  $w_0 = 2/3$  and  $w_1 = w_{-1} = 1/6$  for the equilibrium distribution in the form (18). From (28), the initial populations are obtained in the form

$$\begin{aligned} \tilde{N}_0(x, t) &= \tilde{\rho}_0 w_0 + A w_0 e^{ikx}, \\ \tilde{N}_1(x - c_1 \Delta t, t) &= \tilde{\rho}_0 w_1 + A w_1 e^{ik(x-h)} + \frac{\tilde{\rho}_0 w_1}{\tilde{\theta}} B e^{ik(x-h)}, \\ \tilde{N}_{-1}(x - c_{-1} \Delta t, t) &= \tilde{\rho}_0 w_1 + A w_1 e^{ik(x+h)} - \frac{\tilde{\rho}_0 w_1}{\tilde{\theta}} B e^{ik(x+h)}. \end{aligned} \tag{29}$$

The first step of the LBE algorithm is the calculations of the changes of the initial populations (29) because of the forces between the nodes. In one-dimensional isothermal case, one can obtain from (22)

$$\tilde{\nabla} \tilde{U} = \frac{\partial \tilde{U}}{\partial \tilde{x}} = \left( \frac{\partial \tilde{U}}{\partial \tilde{\rho}} \right)_T \frac{\partial \tilde{\rho}}{\partial \tilde{x}} = R \frac{\partial \tilde{\rho}}{\partial \tilde{x}}, \quad (30)$$

where  $R = k(\partial \tilde{P} / \partial \tilde{\rho})_T - \tilde{\theta}$ . For the finite difference approximation (24) at  $A = 0.5$  (simplest case), we have

$$\tilde{F} = -R \frac{\tilde{\rho}(x+h, t) - \tilde{\rho}(x-h, t)}{2}. \quad (31)$$

For all other finite difference approximations of the force acting on the node, including approximation (24) at different values of free parameter  $A$ , the final expressions in the linear approximation with respect to small amplitude perturbations are the same as (31). Indeed, the numerical simulations show that the criterion of stability does not depend on the specific approximation of the gradient of the potential  $\tilde{U}$ . Hence, the reduced velocity change can be obtained from (21) with the use of (31)

$$\Delta \tilde{u}(x) = \tilde{F} / \tilde{\rho}_0 = -\frac{R}{2\tilde{\rho}_0} A (e^{ik(x+h)} - e^{ik(x-h)}). \quad (32)$$

From (20) and (28), the corresponding changes of the distribution functions can be obtained in the linear approximation  $\Delta \tilde{N}_k = \tilde{\rho}_0 w_k (\tilde{\mathbf{c}}_k \Delta \tilde{\mathbf{u}}) / \tilde{\theta}$  in the form

$$\begin{aligned} \Delta \tilde{N}_0(x) &= 0, \\ \Delta \tilde{N}_1(x - c_1 \Delta t) &= -\frac{w_1 R}{2\tilde{\theta}} A (e^{ikx} - e^{ik(x-2h)}), \\ \Delta \tilde{N}_{-1}(x - c_{-1} \Delta t) &= \frac{w_1 R}{2\tilde{\theta}} A (e^{ik(x+2h)} - e^{ikx}). \end{aligned} \quad (33)$$

Thus, after the first step of the LBE algorithm, the following values of the populations  $\tilde{N}_k^*$  are obtained:

$$\begin{aligned} \tilde{N}_0^*(x, t) &= \tilde{\rho}_0 w_0 + A w_0 e^{ikx}, \\ \tilde{N}_1^*(x - c_1 \Delta t, t) &= \tilde{\rho}_0 w_1 + A w_1 e^{ik(x-h)} + \frac{\tilde{\rho}_0 w_1}{\tilde{\theta}} B e^{ik(x-h)} - \frac{w_1 R}{2\tilde{\theta}} A (e^{ikx} - e^{ik(x-2h)}), \\ \tilde{N}_{-1}^*(x - c_{-1} \Delta t, t) &= \tilde{\rho}_0 w_1 + A w_1 e^{ik(x+h)} - \frac{\tilde{\rho}_0 w_1}{\tilde{\theta}} B e^{ik(x+h)} + \frac{w_1 R}{2\tilde{\theta}} A (e^{ik(x+2h)} - e^{ikx}). \end{aligned} \quad (34)$$

The second step of the LBE algorithm is the advection step

$$\tilde{N}_k(x, t + \Delta t) = \tilde{N}_k^*(x - c_k \Delta t, t). \quad (35)$$

After this step, the distribution of populations at the point  $x$  has the form

$$\begin{aligned} \tilde{N}_0(x, t + \Delta t) &= \tilde{\rho}_0 w_0 + A w_0 e^{ikx}, \\ \tilde{N}_1(x, t + \Delta t) &= \tilde{\rho}_0 w_1 + A w_1 e^{ik(x-h)} + \frac{\tilde{\rho}_0 w_1}{\tilde{\theta}} B e^{ik(x-h)} - \frac{w_1 R}{2\tilde{\theta}} A (e^{ikx} - e^{ik(x-2h)}), \\ \tilde{N}_{-1}(x, t + \Delta t) &= \tilde{\rho}_0 w_1 + A w_1 e^{ik(x+h)} - \frac{\tilde{\rho}_0 w_1}{\tilde{\theta}} B e^{ik(x+h)} + \frac{w_1 R}{2\tilde{\theta}} A (e^{ik(x+2h)} - e^{ikx}). \end{aligned} \quad (36)$$

The third step of the LBE algorithm is the “collision” step. The BGK operator of the “collision” step does not change the new values of density  $\tilde{\rho}(x, t + \Delta t)$  and velocity  $\tilde{u}(x, t + \Delta t)$  at the node.

Therefore, the new values of density and velocity at the point  $x = 0$  are found from (19) and (36):

$$\tilde{\rho}(0, t + \Delta t) = \tilde{\rho}_0 + w_0 A + 2w_1 A \cos kh + \frac{w_1 R A}{\tilde{\theta}} (\cos 2kh - 1) - i \frac{2\tilde{\rho}_0 w_1}{\tilde{\theta}} B \sin kh, \quad (37)$$

$$\tilde{u}(0, t + \Delta t) = -i \frac{2w_1 A}{\tilde{\rho}_0} \left( \sin kh + \frac{R}{2\tilde{\theta}} \sin 2kh \right) + \frac{2w_1}{\tilde{\theta}} B \cos kh. \quad (38)$$

Thus, the transition matrix  $G$  for our variant of the LBE method can be written in the form

$$G = \begin{pmatrix} w_0 + 2w_1 \cos kh + \frac{w_1}{\tilde{\theta}} (\cos 2kh - 1) R & -i \frac{2w_1 \tilde{\rho}_0}{\tilde{\theta}} \sin kh \\ -i \frac{2w_1}{\tilde{\rho}_0} \left( \sin kh + \frac{R}{2\tilde{\theta}} \sin 2kh \right) & \frac{2w_1}{\tilde{\theta}} \cos kh \end{pmatrix}. \quad (39)$$

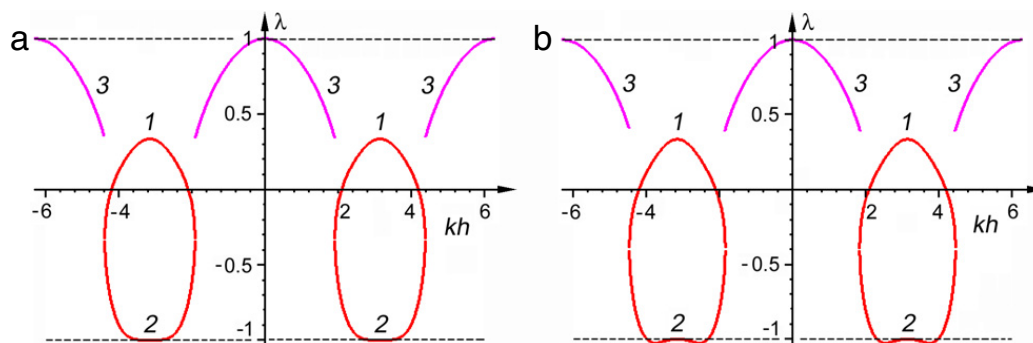


Fig. 6. Eigenvalues of the transition matrix  $G$  versus  $kh$  for  $\tilde{\theta} = 1/3$ ,  $R = 1$  (a), 1.2 (b).

The corresponding eigenvalue equation

$$\lambda^2 - \lambda \left( w_0 + 2w_1 \cos kh + \frac{w_1}{\tilde{\theta}} (\cos 2kh - 1)R + \frac{2w_1}{\tilde{\theta}} \cos kh \right) + \left( w_0 + 2w_1 \cos kh + \frac{w_1}{\tilde{\theta}} (\cos 2kh - 1)R \right) \frac{2w_1}{\tilde{\theta}} \cos kh + \frac{4w_1^2}{\tilde{\theta}} \sin kh \left( \sin kh + \frac{R}{2\tilde{\theta}} \sin 2kh \right) = 0 \quad (40)$$

is quadratic and has two roots.

In the case  $R \leq 1$ , the moduli of both roots of the eigenvalue equation are not greater than unity (Fig. 6(a)). Indeed, the second root  $\lambda_2$  (curve 2) can be expanded in the series  $\lambda_2 = -1 + \frac{3}{4}(1-R)(kh - \pi)^2 + O((kh - \pi)^4)$  in the vicinity of the value  $kh = \pi$  at  $\tilde{\theta} = 1/3$ . If  $R > 1$ , then  $\lambda_2 < -1$  in this region and, consequently,  $|\lambda_2| > 1$  (Fig. 6(b)). In a certain range of the values of  $kh$ , the two complex roots are complex-conjugate numbers and have the same modulus. This modulus is shown in Fig. 6 (curve 3) for  $\tilde{\theta} = 1/3$ .

Another set of equilibrium populations  $N_k^{\text{eq}}(\rho, \mathbf{u}, \theta)$  was proposed in [17], for which the dimensionless kinetic temperature can be varied in the range  $0 < \tilde{\theta} < 1$ . The coefficients are  $w_0 = 1 - \tilde{\theta}$  and  $w_1 = w_{-1} = \tilde{\theta}/2$  in this case. For  $\tilde{\theta} = 1/3$ , this distribution exactly coincides with distribution (5) for the D1Q3 model. The modulus of the complex roots is found from (40) and is equal to  $|\lambda| = \sqrt{\tilde{\theta} + \cos kh(1 - \tilde{\theta})}$ . It is remarkable that this expression does not depend on  $R$ . Obviously,  $\tilde{\theta} + \cos kh(1 - \tilde{\theta}) \leq 1$  for all values of the kinetic temperature  $0 < \tilde{\theta} < 1$ .

Thus, the criterion of numerical stability of the LBE algorithm is obtained in the form  $R = k(\partial \tilde{P} / \partial \tilde{\rho})_T - \tilde{\theta} \leq 1$ . If one substitutes the hydrodynamic Courant number squared  $\tilde{c}^2 = k(\partial \tilde{P} / \partial \tilde{\rho})_T$  into this criterion, then criterion (26) is obtained.

## References

- [1] X. Shan, H. Chen, Lattice Boltzmann model for simulating flows with multiple phases and components, *Phys. Rev. E* 47 (3) (1993) 1815–1819.
- [2] R. Zhang, H. Chen, Lattice Boltzmann method for simulations of liquid–vapor thermal flows, *Phys. Rev. E* 67 (6) (2003) 066711.
- [3] P. Yuan, L. Schaefer, Equations of state in a lattice Boltzmann model, *Phys. Fluids* 18 (4) (2006) 042101.
- [4] M.R. Swift, W.R. Osborn, J.M. Yeomans, Lattice Boltzmann simulation of nonideal fluids, *Phys. Rev. Lett.* 75 (5) (1995) 830–833.
- [5] J. Zhang, B. Li, D.Y. Kwok, Mean-field free-energy approach to the lattice Boltzmann method for liquid–vapor and solid–fluid interfaces, *Phys. Rev. E* 69 (3) (2004) 032602.
- [6] A.L. Kupershtokh, D.A. Medvedev, D.I. Karpov, On equations of state in a lattice Boltzmann method, *Comput. Math. Appl.* 58 (5) (2009) 965–974.
- [7] A.L. Kupershtokh, New method of incorporating a body force term into the lattice Boltzmann equation, in: *Proc. 5th International EHD Workshop*, University of Poitiers, Poitiers, France, 2004, pp. 241–246.
- [8] A.L. Kupershtokh, D.I. Karpov, D.A. Medvedev, C.P. Stamatelatos, V.P. Charalambakos, E.C. Pyrgioti, D.P. Agoris, Stochastic models of partial discharge activity in solid and liquid dielectrics, *IET Sci. Meas. Technol.* 1 (6) (2007) 303–311.
- [9] A.L. Kupershtokh, Simulation of flows with liquid–vapor interfaces by the lattice Boltzmann method, *Vestnik NGU (Quart. J. of Novosibirsk State Univ., Ser.: Math. Mech. Inform.)* 5 (3) (2005) 29–42 (in Russian).
- [10] A.L. Kupershtokh, Calculations of the action of electric forces in the lattice Boltzmann equation method using the difference of equilibrium distribution functions, in: *Proc. 7th Int. Conf. on Modern Problems of Electrophysics and Electrohydrodynamics of Liquids*, St. Petersburg State University, St. Petersburg, Russia, 2003, pp. 152–155.
- [11] Y.H. Qian, D. d’Humières, P. Lallemand, Lattice BGK models for Navier–Stokes equation, *Europhys. Lett.* 17 (6) (1992) 479–484.
- [12] X. He, X. Shan, G.D. Doolen, Discrete Boltzmann equation model for nonideal gases, *Phys. Rev. E* 57 (1) (1998) R13–R16.
- [13] L.-S. Luo, Unified theory of lattice Boltzmann models for nonideal gases, *Phys. Rev. Lett.* 81 (8) (1998) 1618–1621.
- [14] I. Ginzburg, P.M. Adler, Boundary flow condition analysis for the three-dimensional lattice Boltzmann model, *J. Phys. II France* 4 (2) (1994) 191–214.
- [15] R.D. Richtmyer, K.W. Morton, *Difference Methods for Initial-Value Problems*, Interscience publisher John Wiley & Sons, 1967.
- [16] P.J. Roache, *Computational Fluid Dynamics*, Hermosa Publishers, Albuquerque, New Mexico, 1972.
- [17] N.I. Prasianakis, I.V. Karlin, Lattice Boltzmann method for thermal flow simulation on standard lattices, *Phys. Rev. E* 76 (1) (2007) 016702.